Vol.4, No.9, Page 2441- 2449, 2026 https://doi.org/10.59628/jast.v4i9.3005 ISSN 2958-9568 JAST

SUN PUBLISHER

مجلة جامعة صنعاء للعلوم التطبيقية والتكنولوجيا

Sana'a University Journal of Applied Sciences and Technology

https://journals.su.edu.ye/index.php/jast/

Influence of Nano Cu_2O additions on some physical properties of Sn-9Zn melt-spun solder alloy

Ahmed Al-jarbani * and Shakib Alsowidy

Department of Physics, Faculty of Sciences, Sana'a University, Sana'a, Yemen

*Corresponding author: ahmed395a@gmail.com

Abstract

X-ray diffraction (XRD), scanning electron microscopy (SEM), differential scanning calorimetry (DSC), and surface deformation resistance (Vickers hardness HV) measurements have been used to examine the influence of Cu_2O nanoparticles on some physical characteristics of the Sn-9Zn eutectic melt-spun solder alloy at various concentrations of 0, 0.5, 1, 2.5, and 5 wt.%. Five compositions of Sn-9 wt.% Zn-x wt.% Cu_2O (x = 0, 0.5, 1, 2.5, and 5) were prepared from Sn, Zn elements, and Cu_2O nanoparticles with a purity of 99.99% using melt-spinning method. XRD and SEM results indicated that adding Cu_2O nanoparticles to the Sn-9Zn solder alloy produces a fine and high homogeneity microstructure. This is due to the grain boundary pinning effect by Cu_2O nanoparticles, which are dispersed in the solder matrix, causing a uniform microstructure. DSC results exhibited that, as more Cu_2O nanoparticles were added, thermal stability and a higher melting temperature were observed. Vickers hardness (HV) examinations showed that, Cu_2O additives enhance the surface resistance for the plastic indentation with different loads. Just as with 25 gf, the smallest value is 5.5 HV without Cu_2O content, while the highest value is 14.8 HV at 1 wt.% Cu_2O content. This observation is because Cu_2O nanoparticles increase structure density, which agrees with the SEM results.

Article Info

Keywords:
Eutectic Sn-9Zn, Cu_2O nanoparticles, Melt-spun process, Microstructure stability, Thermal properties, Vickers hardness.

Article History:
Received: 18-April-2026,
Revised: 19-May-2026,
Accepted: 01-August-2026,
Published: 28 September 2026.

1. INTRODUCTION

conventional Sn-Pb solder alloys are inexpensive, have a low melting point, and are wettable; therefore, they are widely used as standard materials for electronic packaging [1]. Owing to the toxic nature of Pb, finding appropriate Pb-free solders to replace traditional Sn-Pb eutectic alloys has been a priority [2–4]. Lead-free solder alloys are typically Sn-based because of the high corrosion resistance and good solderability of tin (Sn) [5]. To use lead-free solder alloys as soldering materials, they must satisfy several requirements, including affordability, good wettability, appropriate melting temperature for soft and hard work, superior mechanical and electrical conductivity, strong corrosion resistance, and eco-friendliness [6]. Sn/Zn lead-free solder is a conventional alternative to the toxic Sn/Pb alloy. It has a low melting point, is inexpensive, non-toxic, and structurally stable. However, owing to its high sensitivity to oxygen and susceptibility to corrosion, the application of Sn-Zn solder is restricted [7]. Solder containing zinc has a very low oxidation resistance because zinc readily reacts with oxygen [8]. The flow of molten Sn-Zn solder is impeded, and the oxide coating formed when zinc and oxygen atoms react diminishes the filling ability of the liquid solder. Therefore, one of the primary ways to enhance the performance of the solder is to increase its oxidation resistance by adding a third element [9]. This has led to more extensive research on the development of Sn-9Zn alloys. Recent studies have focused on strengthening lead-free solders with nano- and microalloying to increase their performance [10, 11]. Nanoparticles have a major impact on lead-free solder wettability, mechanical properties, and grain refinement because of their superior physicochemical properties and size effects [12–17]. The high surface energy and large unique surface area of the nanoparticles provide nucleation sites during the solidification of the solder. This may alter the microstructure of the composite solder

©2026 The Author(s). This article is licensed under CC By 4.0

and provide additional grain boundaries that serve as corrosion-resistant barriers [18]. It has been found that the Sn-9Zn solder alloy's microstructural characteristics and overall performance are greatly improved by the size and distribution of Cu_2O nanoparticles. By adding these nanoparticles, the mechanical properties of the solder are greatly improved, particularly its strength and hardness, which increases the solder's resistance to deformation under stress [19]. The microstructure of the Sn-9Zn solder alloy was significantly altered by the inclusion of Cu_2O nanoparticles. These nanoparticles enhance the thermal and mechanical characteristics of the alloy by facilitating microstructural refinement [20]. The wettability of the Sn-9Zn solder alloy was significantly influenced by the addition of Cu_2O nanoparticles. Studies have shown that adding 1 wt. % of Al_2O_3 nanoparticles combined with Cu_2O can reinforce wettability by up to 96.9% [21]. Although Cu_2O nanoparticles have demonstrated the ability to stabilize the alloy against oxidation, the need to strike a balance between enhancing oxidation resistance and preserving wettability remains the most important issue [22]. R. Afify Ismail et al. [23] studied the effect of nanoparticles on the microstructure and mechanical properties of a Sn-Zn solder alloy; they found that the uniform dispersion of nanosized reinforced particles in the solder matrix caused microstructure refinement when 1 wt. % of either CuO or TiO_2 was added. Xing et al. [24] studied the effect of nanosized Al_2O_3 particles on the mechanical and microstructural properties of a Sn-9Zn solder alloy. They concluded that Al_2O_3 enhanced the overall strength of the composite solder. Al-Ganainy et al. [25] studied the effects of ZnO nanoparticles on the thermal, microstructural, and tensile creep properties of Sn-6.5Zn-3In solder alloy. They found that the size of β-Sn dendrites could be considerably reduced by adding a tiny amount of ZnO nanoparticles. The dispersion of ZnO on the grain surface, which lowers the growth rate of β-Sn grains, is responsible for this refining. This is due to the pinning action of ZnO and dispersion strengthening. Gain et al. [26] studied the effects of Ag nanoparticles on the microstructure and shear strength of a Sn-9Zn solder alloy. They discovered that Ag nanoparticles combined with Sn atoms to create a spherical Ag_3Sn IMC phase, which enhanced the mechanical characteristics and refined the solder matrix phase. Zhang et al. [27] studied the effects of Ag and Ni nanoparticles on the microstructure and thermal properties of a Sn-8Zn-Bi solder alloy. They found that adding Ag and Ni nanoparticles successfully stopped the growth of IMC in the structure. As the Zn-Ni IMC and Ni nanoparticles increased the number of heterogeneous nucleation sites, they might also restrict the grain growth of the α-Zn phase. According to Hu et al. [28], the wettability of Sn-Zn solder can be enhanced by including a trace amount of rare-earth Nd. This is surface active. This can enhance the ability of liquid solder to flow at low temperatures and lower the solder surface tension. Xing et al. [18] examined the impact of Al_2O_3 nanoparticles on the microstructure of Sn-Zn solder. The results demonstrated that the addition of nanoparticles to the β-Sn matrix led to a more homogeneous and finer microstructure for the Sn-Zn eutectic. Al_2O_3 nanoparticles can refine the grains of the solder composite and prevent the formation of coarse dendritic Sn-Zn eutectic structures. Shen et al. [29] investigated the impact of adding nanomaterials on the mechanical characteristics of Sn-Zn solder junctions. The findings demonstrated that adding ZrO_2 nanoparticles significantly enhanced the mechanical characteristics of the solder connections. Because of their small size, ZrO_2 nanoparticles can be incorporated into the solder matrix to pin the grain boundaries. To a certain degree, ZrO_2 particles can prevent dislocations from occurring, increasing the shear strength of the solder joint when subjected to external stress. Huang et al. [30] investigated the influence of nano-SiC on the wettability and microstructure of a Sn-9Zn eutectic alloy. The results demonstrate that adding nano-SiC refines the alloy microstructure via grain boundary strengthening and dispersion strengthening, thereby improving the microhardness. Al Hashedi et al. [31] investigated the effects of incorporating CuO nanoparticles (NPs) on the microstructure, mechanical, thermal, and electrical properties of Sn-10Zn solder alloys. The findings demonstrated that the inclusion of CuO NPs was an effective strategy for enhancing the performance of new lead-free solder alloys, offering improved mechanical, thermal, and electrical properties of the solder alloys. Mohamed et al. [32]. investigated the effects of incorporating ZrO_2 or Ni nanoparticles on the microstructure, electrical properties, and hardness of an advanced Sn-9Zn alloy. The results revealed that the inclusion of ZrO_2 reduced the unit cell volume of β-Sn with a contraction in the lattice parameters, which refined the crystallite size and reduced the β-Sn grain size, thereby improving the hardness. The mechanical, thermal, and physical properties of solder formulations are improved by the incorporation of nanoparticles, making them suitable for the increasingly complex needs of contemporary electronic devices [33]. Although several studies have investigated the effects of various nanoparticles on the microstructure and properties of Sn-9Zn solder alloys, the combined effect of nanoparticles and rapid solidification via melt spinning remains limited. The novelty of this work lies in combining Cu_2O nanoparticle reinforcement with melt spinning processing and establishing a direct relationship between crystallite size, structure refinement, thermal behavior, and hardness as a function of Cu_2O concentration. Therefore, this experimental study attempts to improve the mechanical resistance and performance of the melt-spun Sn-9Zn common solder alloy through a series of microstructural modifications, including small additions of Cu_2O nanoparticles.

©2026 The Author(s). This article is licensed under CC By 4.0

2. MATERIALS AND METHODS

Various concentrations of Cu_2O nanoparticles (0, 0.5, 1, 2.5, and 5 wt. %) were chosen for doping the Sn-9Zn eutectic alloy. These lead-free solder alloys were made using 99.99% pure Sn, Zn, and Cu_2O nanoparticles, as indicated in Table (1). The weighted elements were mixed and melted at approximately $450\,^{\circ}\mathrm{C}$ in a vacuum electric furnace within a porcelain crucible for **30** min. Afterwards, the molten solder alloys were agitated to improve homogeneity before being put back in the furnace for another **15** min. Then, the molten solder alloys were poured on a copper roller of the melt-spinning technique, which rotated at a linear speed of 31.4 m/s [34]. The formula R = (t × v/d) was used to determine the solidification rate (R), where (t) is the thickness of the sheet, **(**v**)** is the surface velocity of the copper wheel, and **(**d**)** is the distance between the surface of the copper wheel and the crucible nozzle. Rapid solidification is required for material softening, refined and non-equilibrium crystallite size in material processing, and elimination of micro-segregation up to the amorphous state. This is an attempt to apply these benefits to the soldering process [35]. The resulting samples were long ribbons with a thickness of approximately $70\,\mu\mathrm{m}$.

Table 1. Chemical compositions of Sn-9Zn-XCu2O alloys

Chemical compositions in wt.%				
Alloy	Sample	Sn	Zn	Cu_2O
Sn-9Zn	S1	91	9	0
Sn-9Zn-0.5Cu_2O	S2	90.545	8.955	0.5
Sn-9Zn-1Cu_2O	S3	90.09	8.91	1
Sn-9Zn-2.5Cu_2O	S4	88.725	8.775	2.5
Sn-9Zn-5Cu_2O	S5	86.45	8.55	5

The X-ray Shimadzu EDX-720 model with CuKα radiation (λ = 1.54056) and a scanning electron microscope (SEM) of the type JEOL JSM-6510 LV (Japan) that operates at 30 KV with a high resolution of 3 nm were used to study the phase structure and morphology of the samples. The variation in the heat flow rate as a function of the heating temperature was investigated for the five samples using differential scanning calorimetry (DSC) with an SDT Q600 device (USA) at a heating rate of $10\,\mathrm{K\,min^{-1}}$. Microhardness measurements were conducted on the melt-spun ribbons of Sn-9Zn-xCu_2O alloys using a Vickers hardness tester (FM7- Tech Group„ TokyoJapan) under three different loads (25, 50, and 100 gram-force (gf)) at room temperature for dwell times of 5 s and 90 s.

3. RESULTS AND DISCUSSION

3.1. Structural analysis

Duwez et al. [36] were the first researchers to use rapid cooling for melting alloys. They observed that rapid solidification produces benefits such as increased solid solubility and non-equilibrium phases or amorphous alloys.

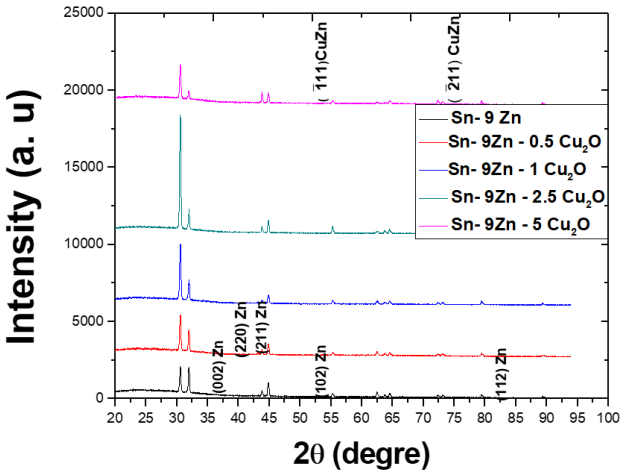


Figure 1. XRD patterns of Sn-9Zn-xCu2O alloys

The X-ray diffraction patterns of Sn-9Zn-x Cu_2O melt-spun solder alloys with x = 0, 0.5, 1, 2.5, and 5 wt. % are shown in Fig. 1. There are many peaks representing the β-Sn and α-Zn phases and few peaks for the CuZn IMC phase. Patterns in Fig. 1 showed that the Sn-9Zn binary melt-spun alloy has three peaks for the α-Zn phase, while the composition Sn-9Zn-0.5wt. % Cu_2O has two peaks for α-Zn. This indicates that Zn exists as a separate phase in these melt-spun alloys because the percentage of nano-oxide was insufficient to alter the zinc atom distribution in the alloy. In addition, there are no α-Zn peaks at high Cu_2O concentrations (1, 2.5, and 5 wt. %); this may be due to some Zn atoms dissolving in the β-Sn matrix phase and some reacting with Cu atoms to produce new compounds. The practical usage of the Sn-9Zn solder alloy is limited because of the significant reduction in oxidation resistance caused by the presence of the α-Zn phase [37]. Our study found that adding Cu_2O to the Sn-9Zn alloy produced a more homogeneous microstructure with a lower volume fraction of the Zn rods phase. Nanoparticles of Cu_2O act as nucleation points, preventing uniform growth and segregation of the α-Zn phase, and causing a more homogenous crystalline structure [18]. Also, it can be observed from the patterns in Fig. 1 The formation of the CuZn IMC phase at 5 wt. % of Cu_2O may be due to the copper content reaching a suitable level to generate a stable intermetallic compound between copper and zinc; this means that Cu_2O nanoparticles have effectively mixed within the Sn-9Zn solder alloy. The XRD details obtained for the Sn-9Zn-

©2026 The Author(s). This article is licensed under CC By 4.0

xCu_2O melt-spun solder alloys are summarized in Table 2.

Table 2. XRD details of Sn-9Zn-xCu2O alloys

Sample	Particle size (D) β-Sn(nm)	Particle size (D) α-Zn(nm)	Particle size (D) CuZn(nm)	(JCPDS-ICDD) Reference
S1	37.75	27.69	——-	β-Sn PDF# 00-004-0673
S2	55.97	84.85	——-	α-Zn PDF#00-004-0831
S3	42.73	——-	——-	
S4	38.43	——-	——-	CuZn PDF#02-1231
S5	40.29	——-	54.16	

The particle sizes of the β-Sn, α-Zn phases, and CuZn IMC were calculated using the Scherrer formula [38]:

$$D = \frac{0.9\,\lambda}{B\,\cos\theta_B} \tag{1}$$

where B is the broadening of the diffraction line measured at half its maximum intensity (radians), D is the diameter of the crystal particle, is the Bragg angle, and λ is the wavelength of the X-ray. Table 2 shows that the crystallite size of β-Sn increased from 37.75 nm without Cu_2O to 55.97 nm at 0.5 wt. % Cu_2O. This percentage of nanoparticles was insufficient to prevent and stop grain growth. At 1 and 2.5 wt.% of Cu_2O, the crystallite size of β-Sn decreases due to the increased effect of grain boundary pinning phenomena. This is because the nano-oxide particles limit the size of the crystals and prohibit further expansion by preventing grain growth, resulting in better structural homogeneity [30]. Adding nanoscale particles to lead-free solder alloys behaves as nucleation centers, which enhances the morphology and creates fine crystalline grains. In addition, the addition of nanoparticles helps decrease the surface tension of the liquid solder and enhances the fluidity and spreading capability of the solder [17, 25, 39]. Adding 5 wt.% copper oxide nanoparticles into the Sn-9Zn base alloy results in a small increase in the crystallite size, as seen in Table 1. It was concluded that adding high concentrations of Cu_2O nanoparticles to the structure permits a small amount of grain growth, producing a coarsening distortion structure. This could be the result of the internally localized concentrated stresses that influence the homogeneity of the alloy by allowing certain crystals to form and reorganize. From XRD patterns in Fig. 1 There are perceivable changes in the entensity of the Sn-9Zn-xCu_2O lead-free alloys, which may be due to the rapid solidification of the melt-spinning technique [34].

3.2. Microstructural analysis

Fig. (2) shows the SEM images of the $Sn-9Zn-xCu_2O$melt-spun solder alloys. From Fig. (2-a), a heterogeneous microstructure along with an irregular phase distribution and visible microstructural flaws are observed. Also, it is clear that the microstructure consists of coarse and elongated grains, as indicated within Fig. (2-a). The nature of this structure affects the wettability and soldering ability of melt-spun alloys. There are two main phases in the microstructure of the Sn-9Zn binary melt-spun alloy, as shown in Fig. (2-a). The two phases are β-Sn and α-Zn, as extracted and obtained from the XRD pattern shown in Fig. 1. (Fig. 2-a) shows two colored regions: the black-gray and white-gray regions. The black-gray region represents the β-Sn matrix phase. This is consistent with the large Sn intensity peaks in the XRD patterns in Fig. 1 and Table 1 respectively. The white-grey region represents the α-Zn particles, which are needle-like rods and small spherical particles, and distributed along the entire microstructure [40]

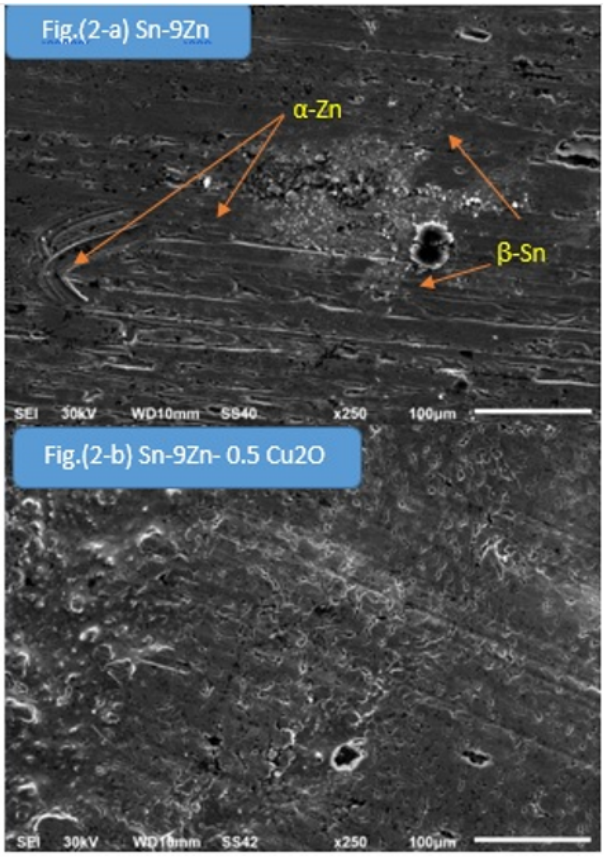


Figure 2. Figs. (2-a and b): SEM images of Sn-9Zn and Sn-9Zn-0.5 Cu_2O alloys.

After adding 0.5 wt.% Cu_2O nanoparticles to the Sn-9Zn binary alloy, the microstructure begins to reduce in size and becomes denser, as seen in Fig.(2-b). The non-uniform distribution of grains, consisting of fine-grained

©2026 The Author(s). This article is licensed under CC By 4.0

areas next to coarse-grained areas, is shown in Fig. (2-b) reflects irregular growth in the microstructure. This irregularity is illustrated in Fig. (2-b) as several spots that represent grains larger than those of the original alloy. From Fig. (2-c), the micrograph shows a very homogeneous structure with small grains and a nearly flawless Sn-Zn phase combination. The micrograph visually reveals a few tiny white particles distributed on the surface of the sample; these particles may be Cu_2O nanoparticles that have not been completely dissolved in the alloy during the manufacturing process. The spherical nature of the grains is evident in all areas, and the dendrite structure begins to nucleate within the microstructure. The flower structure of Zn particles is shown along the lamellar β-Sn and α-Zn subsequence particles, as shown in Fig. (2-c). The flowers and dendrite structures have the highest mechanical strength for localized plastic deformation and durability [41, 42]. Small particles, less than 30 nm, are distributed in various regions of the microstructure, as shown in Fig. (2-c). These particles represent two compounds: CuZn particles and the remaining Cu_2O nanoparticles. Due to the small size of these particles being less than the detection limit for the XRD beam, the XRD pattern exhibited only one type of peak representing the Sn-matrix phases, as shown in Fig. 1.

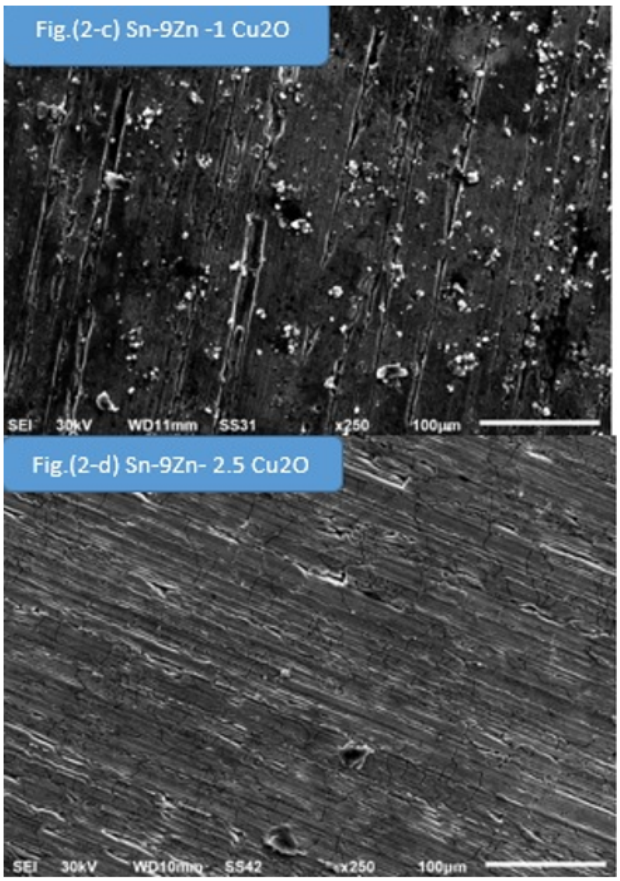


Figure 2. (c and d): SEM images of Sn-9Zn-1 Cu_2O and Sn-9Zn-2.5 Cu_2O alloys.

Fig. (2-d) reveals the regular distribution of Cu_2O nanoparticles, which not only interrupted grain boundary migration but also resulted in a homogeneous microstructure and fine grains. The micrograph also displays small particles on the surface of the alloy as small white regions distributed over the surface of the alloy. This might indicate how the Cu_2O nanoparticles influence the distribution of the secondary phase, act as barriers to grain growth, and may contribute to an increase in the mechanical strength. These Cu_2O nanoparticles concentrated and collected at the grain surfaces and grain boundaries at various orientations, ultimately stopping growth in different orientations and permitting growth in other orientations. This observation is in good agreement with the Poisson's ratio phenomena [43], as shown in Fig. (2-d) and Fig. 1.

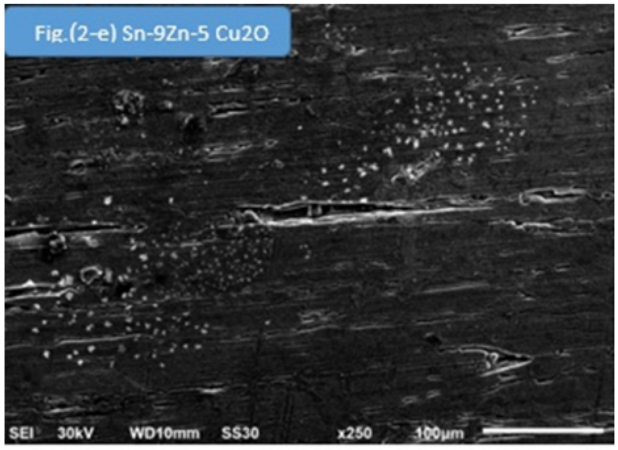


Figure 2. (e): SEM image of Sn-9Zn-5 Cu_2O alloy.

The SEM image in Fig. (2-e) shows a very dense distribution of nanoparticles, indicating that the homogeneity of the alloy may have been affected by the higher particle distribution caused by the high concentration of Cu_2O additives.

3.3. Thermal analysis

The melting temperature is a vital thermal property, and a solder alloy should have a low melting temperature zone [44]. Fig. 3 displays the Differential Scanning Calorimetry (DSC) patterns. While heating the Sn-9Zn-x Cu_2O melt-spun solder alloys, each alloy exhibited a single endothermic peak, confirming one-step melting. The melting behavior of the alloys was investigated using differential scanning calorimetry (DSC) in an argon atmosphere at a heating rate of $10\,\mathrm{k\,min^{-1}}$.

The DSC results are summarized in Table 3. As shown in Table 3, adding Cu_2O nanoparticles to the Sn-9Zn solder alloy increased the melting point (T_m). Table 3 shows that the melting point rises from $206.1\,^{\circ}\mathrm{C}$ without Cu_2O additives to $239.82\,^{\circ}\mathrm{C}$ at 5 wt. % of Cu_2O.

©2026 The Author(s). This article is licensed under CC By 4.0

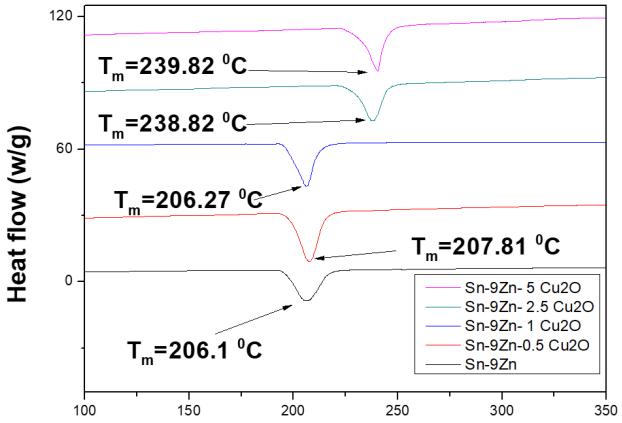


Figure 3. DSC curves of Sn-9Zn-xCu_2O alloys

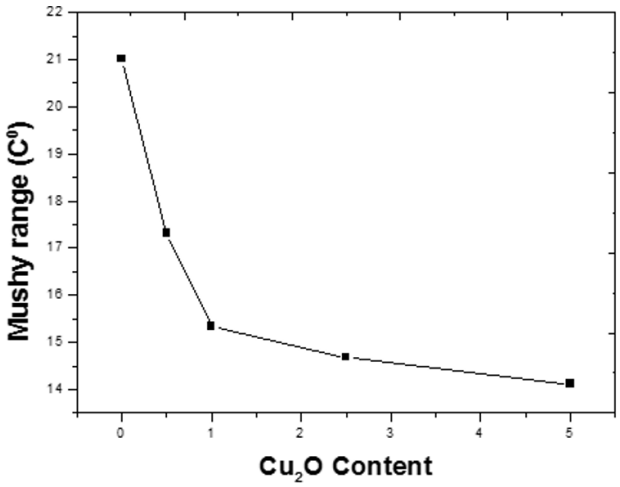


Figure 4. Mushy range versus Cu_2 content

This increase in T_m with the Cu_2O content may be due to Cu_2O the strengthening of the bonds between atoms inside the crystallite structure. This implies greater resistance to localized plastic deformation and corrosion when exposed to high temperatures [45]. The melt-spun technique removes alloys from the equilibrium state [46]. This increase in the melting point is more appropriate for demanding applications. The chemical reaction between Cu_2O molecules and Zn atoms to produce CuZn compounds increased with increasing Cu_2O content. The reduction in the Zn content as a result of the reaction with Cu atoms leads to a shift from the eutectic composition between Sn and Zn and produces a new Sn/Zn hypoeutectic shoulder region. The melting temperature of this hypoeutectic phase is higher than that of the Sn/Zn eutectic phase, as shown in the Sn/Zn phase diagram [47].

Table 3. DSC details of Sn-9Zn-xCu2O alloys

Sample	T_s (° C)	T_m (° C)	T_L (° C)	mushy rang (° C)
S1	195.85	206.10	216.86	21.01
S2	198.15	207.81	215.46	17.31
S3	196.74	206.27	212.08	15.34
S4	228.99	238.82	243.67	14.68
S5	231.29	239.82	245.41	14.12

From the DSC patterns, a small shift between the beginning and end of the phase transition (melting) was noted. The difference between these values represents the pasty (mushy) range, as shown in table 3. The less mushy range observed in the DSC curves with increasing Cu_2O content is shown in Fig. 4 is an indicator of the improvement in mechanical strength and localized plastic deformation.

The small mushy range prevents cracks and segregation in the structure during the soldering process, which makes the alloy suitable for soldering [44].

3.4. Hardness measurements

Vickers hardness (HV) was determined using the follwing formula [48]:

$$H = 1.85\frac{l}{d^2} \quad (2)$$

Where L is the indentation load (g), and d is the mean diagonal of the indentation (mm). Fig. 4 and Table 4 show the Vickers hardness values for the Sn-9Zn melt-spun alloy with the addition of different percentages of Cu_2O nanoparticles (0.5, 1, 2.5, and 5 wt. %). %) under three applied loads (25, 50, and 100 gram force (gf)) and dwell times of 5 and 90 seconds. Fig. (5-a) shows the HV versus Cu_2O content at different applied loads and times. From Fig. (4-a) and Table 4, the HV values gradually increase with increasing Cu_2O content up to 1 wt. % Cu_2O at two times, then it decreases slightly with further increase in Cu_2O content . This is consistent with the results of the thermal analysis shown in Fig. 3 Before and after 1 wt. % Cu_2O. The nanoparticles are distributed within the alloy structure and act as mechanical barriers, inhibiting grain growth and increasing the structural homogeneity. This phenomenon is due to the increased impedance for dislocation movement as more Cu_2O nanoparticles are added and distributed over the grains and grain boundaries. This is consistent with the findings of a previous study [19].

The DSC curves in Fig. 3 revealed two sections above and below the transition composition: Sn-9 wt. % Zn-1 wt.% Cu_2O and Sn-9 wt.% Zn-2.5 wt.% Cu_2O . These compositions have transformation temperatures ranging from 206.1 °C to 238.82 °C at 2.5 wt.% Cu_2O . High Cu_2O content can lead to differences in mechanical strength and hardness. El-Daly et al. [49, 50] demonstrated the effect of the transition temperature on the mechanical strength of certain solder alloys, such as Pb–10 wt. % Sn. The influence of the applied stresses on the HV was extracted from Fig. (5-a) and re-plotted in Fig. (5-b). From Fig. (5-b) and Table 4, the hardness values of the

©2026 The Author(s). This article is licensed under CC By 4.0

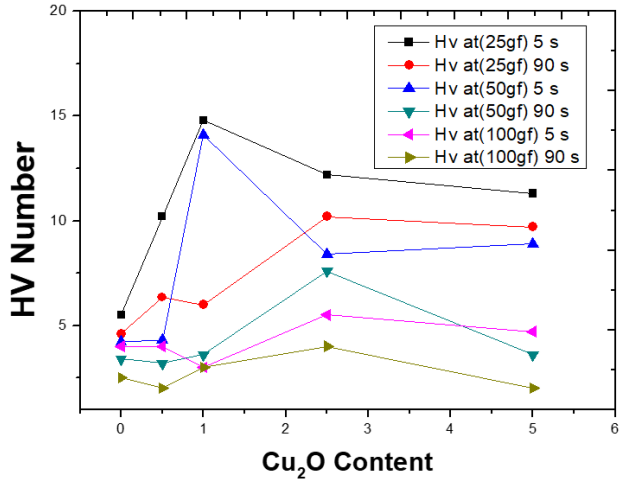


Figure 5. (5-a): HV numbers versus Cu_2O content.

alloy decreased with increasing applied load. This is because high loads may lead to the collapse of the microstructure or breaking of the bonds between particles, and the hardness values appear lower, while at low loads, the effect of the bonding force appears more clearly, and the hardness values are higher [51].

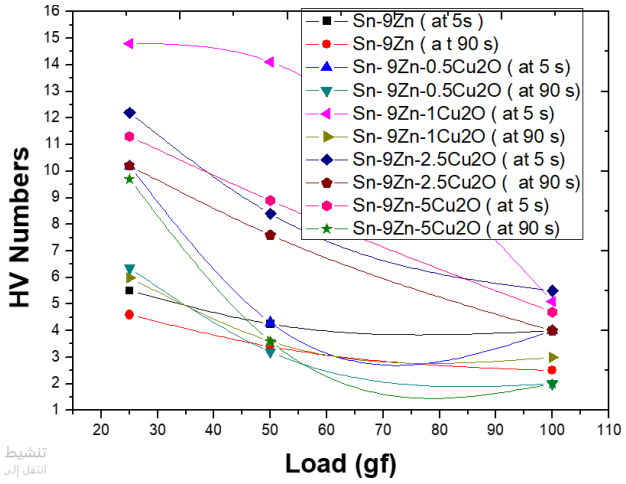


Figure 5. (5-b): HV numbers versus loads.

The effects of the two indentation times, 5 s and 90 s, on the hardness behavior were also examined at the same three applied stresses. The results obtained are tabulated in Table 4, where the strong effect of the indentation time is clear. From Table 4, it can be concluded that the HV number decreases with increasing indentation time from 5 s to 90 s. This means that the sample subjected to applied loads for a long time exhibited less surface resistance to plastic deformation.

4. CONCLUSIONS

The results of this investigation revealed the strong effect of Cu_2Onanoparticle addition on the microstructure and mechanical properties of the Sn-9Zn melt-spun solder alloy.

Table 4. Vickers Hardness (HV) numbers of Sn-9Zn-xCu_2O alloys

Vickers Hardness (HV) numbers			
Sample	Load (gf)	Time	
		5 S	90 S
S1	25	5.5	4.6
	50	4.25	3.4
	100	4	2.5
S2	25	10.2	6.3
	50	4.3	3.2
	100	4	2
S3	25	14.8	6
	50	14.1	3.6
	100	5.1	3
S4	25	12.2	10.2
	50	8.4	7.6
	100	5.5	4
S5	25	11.3	9.7
	50	8.9	3.6
	100	4.7	2.1

• Adding Cu_2O nanoparticles to the Sn-9Zn melt-spun alloy at various concentrations resulted in variations in the crystallite size.

• SEM images showed that the addition of Cu_2O nanoparticles produced fine microstructural homogeneity and uniform grain dispersion.

• The DCS results revealed that the addition of Cu_2O nanoparticles enhanced the heat stability, increased the melting point from 206.1 °C to 239.82 °C, and stabilized the alloy phases.

• HV results showed that the addition of Cu_2O nanoparticles at different concentrations improved the mechanical strength of the alloys. At 25 gf, the smallest value was 5.5 HV without Cu_2O content, whereas the highest value was 14.8 HV at 1 wt. % Cu_2O content.

Overall, adding Cu_2O nanoparticles to the melt-spun Sn-9Zn solder alloy produced a solder alloy with enhanced mechanical and thermal reliability, making it suitable for electronic applications.

REFERENCES

[1] C.-P. Lin, C.-M. Chen, Y.-W. Yen, H.-J. Wu, and S.-W. Chen, "Interfacial reactions between high-pb solders and ag," *J.*

©2026 The Author(s). This article is licensed under CC By 4.0

Alloy. Compd., vol. 509, no. 8, pp. 3509–3514, 2011. DOI: 10.1016/j.jallcom.2010.11.145

[2] B. H.-L. Chao, X. Zhang, S.-H. Chae, and P. S. Ho, "Recent advances on kinetic analysis of electromigration enhanced intermetallic growth and damage formation in pb-free solder joints," *Microelectron. Reliab.*, vol. 49, no. 3, pp. 253–263, 2009. DOI: 10.1016/j.microrel.2008.11.002

[3] J. Shen and Y. C. Chan, "Research advances in nano-composite solders," *Microelectron. Reliab.*, vol. 49, no. 3, pp. 223–234, 2009. DOI: 10.1016/j.microrel.2008.11.003

[4] Y.-W. Wang, Y. W. Lin, and C. R. Kao, "Kirkendall voids formation in the reaction between ni-doped snag lead-free solders and different cu substrates," *Microelectron. Reliab.*, vol. 49, no. 3, pp. 248–252, 2009. DOI: 10.1016/j.microrel.2008.11.007

[5] S. Farina and C. Morando, "Comparative corrosion behaviour of different sn-based solder alloys," *J. Mater. Sci. Mater. Electron.*, vol. 26, no. 1, pp. 464–471, 2015. DOI: 10.1007/s10854-014-2422-0

[6] A. K. Gain, T. Fouzder, Y. C. Chan, A. Sharif, N. B. Wong, and W. K. C. Yung, "The influence of addition of al nanoparticles on the microstructure and shear strength of eutectic sn–ag–cu solder on au/ni metallized cu pads," *J. Alloy. Compd.*, vol. 506, no. 1, pp. 216–223, 2010. DOI: 10.1016/j.jallcom.2010.06.123

[7] A. Sharif and Y. C. Chan, "Investigation of interfacial reactions between sn–zn solder with electrolytic ni and electroless ni(p) metallization," *J. Alloy. Compd.*, vol. 440, no. 1–2, pp. 117–121, 2007. DOI: 10.1016/j.jallcom.2006.09.020

[8] M. Abtew and G. Selvaduray, "Lead-free solders in microelectronics," *Mater. Sci. Eng. R: Reports*, vol. 27, no. 5–6, pp. 95–141, 2000. DOI: 10.1016/S0927-796X(00)00010-3

[9] X. Chen, M. Li, X. Ren, and D. Mao, "Effects of alloying elements on the characteristics of sn-zn lead-free solder," in *2005 6th International Conference on Electronic Packaging Technology*, IEEE, 2005, pp. 211–217. DOI: 10.1109/ICEPT.2005.1564675

[10] M. A. Dudek and N. Chawla, "Effect of rare-earth (la, ce, and y) additions on the microstructure and mechanical behavior of sn-3.9ag-0.7cu solder alloy," *Metall. Mater. Trans. A*, vol. 41, no. 3, pp. 610–620, 2010. DOI: 10.1007/s11661-009-0146-1

[11] P. Xue, S.-b. Xue, Y.-f. Shen, F. Long, and H. Zhu, "Wettability and interfacial whiskers of sn–9zn–0.5ga–0.08nd solder with sn, snbi and au/ni coatings," *J. Mater. Sci. Mater. Electron.*, vol. 25, no. 8, pp. 3520–3525, 2014. DOI: 10.1007/s10854-014-2049-1

[12] A. Fawzy, S. A. Sobhy, M. Nassr, M. M. Mousa, and G. Saad, "Tensile creep characteristics of sn-3.5ag-0.5cu (sac355) solder reinforced with nano-metric zno particles," *Mater. Sci. Eng. A*, vol. 603, pp. 1–10, 2014. DOI: 10.1016/j.msea.2014.02.047

[13] M. A. A. M. Salleh, S. D. McDonald, C. M. Gourlay, H. Yasuda, and K. Nogita, "Suppressing of cu6sn5 in tio2 reinforced solder joints after multiple reflow cycles," *Mater. Des.*, vol. 108, pp. 418–428, 2016. DOI: 10.1016/j.matdes.2016.07.036

[14] L. Yi, K. Luo, A. B. Y. Lim, C. Zhong, F. Wu, and Y. C. Chan, "Improving the mechanical performance of sn57.6bi0.4ag solder joints on au/ni/cu pads during aging and electromigration through the addition of tungsten (w) nanoparticles reinforcement," *Mater. Sci. Eng. A*, vol. 669, pp. 291–303, 2016. DOI: 10.1016/j.msea.2016.05.100

[15] Z. Fathian, A. Maleki, and B. Niroumand, "Synthesis and characterization of ceramic nanoparticles reinforced lead-free solder," *Ceram. Int.*, vol. 43, no. 6, pp. 5302–5310, 2017. DOI: 10.1016/j.ceramint.2017.01.072

[16] L. Zhang and K. N. Tu, "Structure and properties of lead-free solders bearing micro and nanoparticles," *Mater. Sci. Eng. R: Reports*, vol. 82, pp. 1–32, 2014. DOI: 10.1016/j.mser.2014.01.001

[17] Y. Huaung, Z. Xiu, G. Wu, Y. Tian, and P. He, "Sn-3.0ag-0.5cu nanocomposite solders reinforced by graphene nanosheets," *J. Mater. Sci. Mater. Electron.*, vol. 27, pp. 6809–6815, 2016. DOI: 10.1007/s10854-016-4631-1

[18] W. Q. Xing et al., "Microstructure and mechanical properties of sn-9zn-xal2o3 nanoparticles (x = 0–1) lead-free solder alloy: First-principles calculation and experimental research," *Mater. Sci. Eng. A*, vol. 678, pp. 252–259, 2016. DOI: 10.1016/j.msea.2016.09.105

[19] M. Z. Yahaya and E. F. Azmi, "Nanoparticle-reinforced solder alloys: A comprehensive review of recent formulation, properties, and mechanical performance," *J. Mater. Res. Technol.*, pp. 3682–3707, 2024. DOI: 10.1016/j.jmrt.2024.07.XXX

[20] M. Drienovsky et al., "Properties of sn-ag-cu solder joints prepared by induction heating," *Adv. Mater. Sci. Eng.*, vol. 2020, p. 1 724 095, 2020. DOI: 10.1155/2020/1724095

[21] W. Xing et al., "Effect of nano al2o3 additions on the interfacial behavior and mechanical properties of eutectic sn-9zn solder on low temperature wetting and soldering of 6061 aluminum alloys," *J. Alloy. Compd.*, vol. 659, pp. 547–582, 2017.

[22] J. Y. Park, S. Lee, Y. Kim, and Y. B. Ryu, "Antimicrobial activity of morphology-controlled cu2o nanoparticles: Oxidation stability under humid and thermal conditions," *Materials*, vol. 17, no. 1, p. 261, 2024. DOI: 10.3390/ma17010261

[23] R. A. Ismail, "An investigation of microstructure and mechanical properties of different nano-particles doped sn-zn lead-free solder alloys," *Arab. J. Nucl. Sci. Appl.*, vol. 53, no. 1, pp. 191–199, 2020. DOI: 10.21608/ajnsa.2019.13962.1223

[24] W. Xing et al., "Microstructure and mechanical properties of sn-9zn-xal2o3 nanoparticles (x = 0–1) lead-free solder alloy: First-principles calculation and experimental research," *Mater. Sci. Eng. A*, vol. 678, pp. 252–259, 2016.

[25] G. S. Al-Ganainy, A. A. El-Daly, A. Fawzy, and N. Hussein, "Effect of adding nanometric ZnO particles on thermal, microstructure and tensile creep properties of Sn-6.5 wt%Zn-3 wt%In solder alloy," *J. Mater. Sci. Mater. Electron.*, vol. 28, pp. 13 303–13 312, 2017. DOI: 10.1007/s10854-017-7166-1

[26] A. K. Gain, Y. C. Chan, A. Sharif, N. B. Wong, and W. K. Yung, "Interfacial microstructure and shear strength of Ag nano particle doped Sn-9Zn solder in ball grid array packages," *Microelectron. Reliab.*, vol. 49, no. 7, pp. 746–753, 2009. DOI: 10.1016/j.microrel.2009.03.003

[27] A. K. Gain and L. Zhang, "Microstructure, thermal analysis and damping properties of Ag and Ni nanoparticles doped Sn-8Zn-3Bi solder on OSP-Cu substrate," *J. Alloy. Compd.*, vol. 617, pp. 779–786, 2014. DOI: 10.1016/j.jallcom.2014.09.068

[28] Y.-h. Hu, S.-b. Xue, H. Wang, H. Ye, Z.-x. Xiao, and L.-l. Gao, "Effects of rare earth element Nd on the solderability and microstructure of Sn–Zn lead-free solder," *J. Mater. Sci. Mater. Electron.*, vol. 22, no. 5, pp. 481–487, 2011. DOI: 10.1007/s10854-010-0163-2

[29] J. Shen and Y. C. Chan, "Effects of ZrO2 nanoparticles on the mechanical properties of Sn-Zn solder joints on Au/Ni/Cu pads," *J. Alloy. Compd.*, vol. 477, no. 1, pp. 552–559, 2009. DOI: 10.1016/j.jallcom.2008.10.072

[30] J. Huang, W. Hu, Y. Tian, L. Yin, H. Zhang, and G. Wang, "Synergistic modification of Sn9Zn solder using nano-SiC-based interface-active multifunctional reinforcements," *Mater. Charact.*, p. 115 784, 2025. DOI: 10.1016/j.matchar.2025.115784

©2026 The Author(s). This article is licensed under CC By 4.0

[31] S. A. Al Hashedi et al., "CuO nanoparticles-driven microstructure evolution and advanced mechanical, thermal, and electrical properties of Sn-10Zn solder alloys," *J. Mater. Eng. Perform.*, vol. 35, no. 2, pp. 2011–2020, 2026. DOI: 10.1007/s11665-025-11672-x

[32] H. S. Mohamed, M. M. Mostafa, and N. M. Mahmoud, "Crystallographic, microstructure, electrical, and hardness characterization of advanced Sn-9Zn-0.5 ZrO2 and Sn-9Zn-xNi lead-free solder alloys," *J. Mater. Sci. Mater. Electron.*, vol. 36, no. 13, p. 784, 2025. DOI: 10.1007/s10854-025-14760-9

[33] M.-l. Li, L. Zhang, N. Jiang, L. Zhang, and S.-j. Zhong, "Materials modification of the lead-free solders incorporated with micro/nano-sized particles: A review," *Mater. & Des.*, vol. 197, p. 109 224, 2021. DOI: 10.1016/j.matdes.2020.109224

[34] M. Kamal and U. Mohammad, "A review: Chill-block melt spin technique, theories & applications," in *Melt Spinning*, Bentham Science Publishers, 2012, pp. 42–69. DOI: 10.2174/9781608051519120101

[35] G. Rosen, J. Avissar, Y. Gefen, and J. Baram, "Centrifuge melt spinning," *J. Phys. E: Sci. Instruments*, vol. 20, no. 5, pp. 571–574, 1987. DOI: 10.1088/0022-3735/20/5/024

[36] P. Duwez, R. H. Willens, and W. J. Klement, "Metastable electron compound in Ag-Ge alloys," *J. Appl. Phys.*, 1960.

[37] X. Peng, S. B. Xue, Y. F. Shen, and Z. Hong, "Interfacial microstructures and mechanical properties of Sn-9Zn-0.5Ga-xNd on Cu substrate with aging treatment," *Mater. Des.*, vol. 60, pp. 1–6, 2014.

[38] B. D. Cullity, *Elements of X-Ray Diffraction*, 2nd ed. Reading: Addison-Wesley, 1978, p. 248.

[39] L. Yang, J. Dai, Y. Zhang, Y. Jing, J. Ge, and H. Lu, "Influence of BaTiO3 nanoparticles addition on microstructure and mechanical properties of Sn-5Bi solder," *J. Electron. Mater.*, vol. 44, pp. 2473–2478, 2015. DOI: 10.1007/s11664-015-3796-3

[40] S. K. Das, A. Sharif, Y. C. Chan, N. B. Wong, and W. K. C. Yung, "Influence of small amount of Al and Cu on the microstructure, microhardness and tensile properties of Sn-9Zn binary eutectic solder alloy," *J. Alloy. Compd.*, vol. 481, no. 1–2, pp. 167–172, 2009. DOI: 10.1016/j.jallcom.2009.03.063

[41] S. Alsowidy, "Localized plastic deformation and microstructure properties of Al/Si alloy improved with Al3Ni compound," *Sana'a Univ. J. Appl. Sci. Technol.*, vol. 1, no. 3, 2023.

[42] S. Alsowidy, O. Humaid, M. S. Gumaan, and B. Al-Asry, "Effect of CuAl2 on the microstructure and hardness of Al-Si-xCu alloys produced by powder metallurgy," *Sana'a Univ. J. Appl. Sci. Technol.*, vol. 1, no. 4, 2023.

[43] W. D. Callister, *Materials Science and Engineering: An Introduction*. John Wiley & Sons, 2006.

[44] R. M. Shalaby, "Effect of silver and indium addition on mechanical properties and indentation creep behavior of rapidly solidified Bi–Sn based lead-free solder alloys," *Mater. Sci. Eng. A*, vol. 560, pp. 86–95, 2013. DOI: 10.1016/j.msea.2012.09.061

[45] M. Zhao, L. Zhang, Z.-Q. Liu, M.-Y. Xiong, and L. Sun, "Structure and properties of Sn–Cu lead-free solders in electronics packaging," *Sci. Technol. Adv. Mater.*, vol. 20, no. 1, pp. 421–444, 2019. DOI: 10.1080/14686996.2019.1591168

[46] R. M. Shalaby, M. Kamal, E. A. M. Ali, and M. S. Gumaan, "Design and properties of new lead-free solder joints using Sn-3.5Ag-Cu solder," *Silicon*, vol. 10, no. 5, pp. 1861–1871, 2018. DOI: 10.1007/s12633-017-9690-2

[47] R. A. Islam, B. Y. Wu, M. O. Alam, Y. C. Chan, and W. Jillek, "Investigations on microhardness of Sn–Zn based lead-free solder alloys as replacement of Sn–Pb solder," *J. Alloy. Compd.*, vol. 392, no. 1–2, pp. 149–158, 2005. DOI: 10.1016/j.jallcom.2004.09.060

[48] G. B. Ghorbal, A. Tricoteaux, A. Thuault, G. Louis, and D. Chicot, "Comparison of conventional knoop and vickers hardness of ceramic materials," *J. Eur. Ceram. Soc.*, vol. 37, no. 6, pp. 2531–2535, 2017. DOI: 10.1016/j.jeurceramsoc.2017.01.014

[49] A. A. El-Daly, A. M. Abdel-Daiem, A. N. Abdel-Rahman, and S. M. Mohammed, "Effect of zn-addition and structural transformation on the creep behaviour of pb–10 wt.% sn alloy," *Mater. Chem. Phys.*, vol. 85, no. 1, pp. 163–170, 2004. DOI: 10.1016/j.matchemphys.2004.01.010 [Online]. Available: https://www.sciencedirect.com/science/article/abs/pii/S0254058404000288

[50] A. A. El-Daly, A. M. Abdel-Daiem, E. A. El-Saadani, A. N. Abdel-Rahman, and S. M. Mohammed, "Time-dependent deformation behaviour of lead-based bearing alloys during transformation," *Mater. Chem. Phys.*, vol. 83, no. 1, pp. 96–103, 2004. DOI: 10.1016/S0254-0584(03)00469-3 [Online]. Available: https://www.sciencedirect.com/science/article/abs/pii/S0254058403004693

[51] O. Uzun, T. Karaaslan, M. Gogebakan, and M. Keskin, "Hardness and microstructural characteristics of rapidly solidified al–8–16 wt.% si alloys," *J. Alloy. Compd.*, vol. 376, no. 1–2, pp. 149–157, 2004. DOI: 10.1016/j.jallcom.2004.01.012 [Online]. Available: https://www.sciencedirect.com/science/article/abs/pii/S0925838804000520

©2026 The Author(s). This article is licensed under CC By 4.0